HHS Public Access

Author manuscript

Nat Genet. Author manuscript; available in PMC 2014 June 01.

Published in final edited form as:

Nat Genet. 2013 December ; 45(12): 1439–1445. doi:10.1038/ng.2822.

ESR1 ligand binding domain mutations in hormone-resistant breast cancer

Weiyi Toy[1], **Yang Shen**[2], **Helen Won**[1], **Bradley Green**[3], **Rita A. Sakr**[4], **Marie Will**[5], **Zhiqiang Li**[1], **Kinisha Gala**[1], **Sean Fanning**[3], **Tari A. King**[4], **Clifford Hudis**[7], **David Chen**[6], **Tetiana Taran**[6], **Gabriel Hortobagyi**[8], **Geoffrey Greene**[3], **Michael Berger**[1,5], **Jose Baselga**[1,5], and **Sarat Chandarlapaty**[1,5,7]

[1]Human Oncology and Pathogenesis Program, Memorial Sloan-Kettering Cancer Center (MSKCC), New York, NY, USA

[2]Toyota Technological Institute at Chicago, Chicago, IL, USA

[3]Ben May Department of Cancer Research, University of Chicago, Chicago, IL, USA

[4]Breast Service, Department of Surgery, MSKCC, New York, NY, USA

[5]Weill Cornell Medical College, New York, NY, USA

[6]Novartis Pharmaceuticals Corporation, East Hanover, NJ, USA

[7]Breast Cancer Medicine Service, Solid Tumor Division, Department of Medicine, MSKCC, New York, NY, USA

[8]Department of Breast Medical Oncology, MD Anderson Cancer Center, Houston, TX, USA

Abstract

Seventy percent of breast cancers express estrogen receptor (ER) and most of these are sensitive to ER inhibition. However, many such tumors become refractory to inhibition of estrogen action in the metastatic setting for unknown reasons. We conducted a comprehensive genetic analysis of two independent cohorts of metastatic ER^+ breast tumors and identified mutations in the ligand binding domain (LBD) of *ESR1* in 14/80 cases. These included highly recurrent mutations p.Tyr537Ser/Asn and p.Asp538Gly. Molecular dynamics simulations suggest the Tyr537Ser and Asp538Gly structures lead to hydrogen bonding of the mutant amino acid with Asp351, thus

Correspondence: Sarat Chandarlapaty, MD, PhD, Human Oncology and Pathogenesis Program, Memorial Sloan-Kettering Cancer Center, 1275 York Ave, New York, NY, 10065 USA, (T) 646-888-3387, chandars@mskcc.org.

Author Contributions

S.C., W.T., Y.S., G.G., J.B., G.H., and M.B. conceived and designed the experiments.
W.T., Y.S., H.W., B.G., S.F., R.A.S., M.W., Z.L., K.G., and S.C. conducted the experiments.
W.T., S.C., Y.S., G.G., M.B., H.W., D.C., T.T., J.B., G.H., T.A.K. and C.H. analyzed the data. W.T., S.C., Y.S., and H.W. wrote the manuscript.

Competing Financial interests

The authors declare no competing financial interests.

Accession codes

Gene expression array data of MCF7 cells transfected with GFP-ERα WT and mutants in this study has been deposited in GEO under the GEO accession GPLxxx.

favoring the receptor's agonist conformation. Consistent with this model, mutant receptors drive ER-dependent transcription and proliferation in the absence of hormone and reduce the efficacy of ER antagonists. These data implicate LBD mutant forms of ER in mediating clinical resistance to hormonal therapy and suggest that more potent ER antagonists may have significant therapeutic benefit.

Introduction

The estrogen receptor (ER) is a member of the nuclear receptor family and regulates the transformed phenotype of the majority of breast cancers. Pharmacologic inhibitors of estrogen driven-signaling are effective in many of these cases[1]. Therapeutics in this class include drugs that suppress estrogen production (aromatase inhibitors, GnRH agonists) and direct inhibitors of the estrogen receptor (selective estrogen receptor modulators (SERM) or selective estrogen receptor degraders (SERD))[2]. Although most patients with ER+ breast cancer derive a benefit from these drugs, resistance often emerges after prolonged exposure[1,3–5]. The mechanisms underlying this phenomenon are unclear and a better understanding of acquired resistance to hormone antagonists is essential for the development of more durable and effective therapy.

Results

ESR1 mutations detected in patients with ER+ metastatic breast cancer

To identify possible genetic mechanisms of acquired resistance to hormonal therapy, we sought to characterize tumors from patients with metastatic ER+ breast cancer treated for at least 3 months with hormonal therapy and whose tumors had grown or spread to new sites while on therapy. As part of a metastatic breast tumor procurement protocol (National Clinical Trials Registry#00897702), we identified 38 (out of 71) samples that met these criteria and had sufficient tumor DNA for analysis. We utilized a targeted approach to genomic characterization surveying for mutations and copy number alterations among 230 genes commonly mutated in cancer by massively parallel sequencing (MSKCC sequencing panel)[6]. Two cases were dropped out of the analysis did not pass quality control testing for being from a single source. Among our cohort, we had normal DNA from white blood cells (WBCs) for comparison in 22 cases. Analysis of these 22 matched samples revealed an average of 4.3 mutations per tumor with a mean coverage depth of ~500X (Normal: 441X, Mets: 696X) (Supplementary Table 1). Among these, 6 genes were mutated in more than 10% of the matched cases. We compared the prevalence of mutations in these genes in our set of relapsed tumors with those in The Cancer Genome Atlas (TCGA) invasive primary (untreated) breast cancer and luminal A/B primary breast cancer cases and found that the prevalence of mutations in *TP53*, *PIK3CA* and *GATA3* were comparable in all sets (Fig. 1a)[7]. By contrast, *ESR1*, *RPTOR* and *ERBB3* mutations were detected at much higher rates in our samples than in those reported by TGCA. That these mutations are enriched among tumors from patients who had relapsed while on hormonal therapy suggests that they may play a role in the development of acquired resistance. Gene copy number was also analyzed in these samples and Figure 1b shows the genes that were frequently amplified. Amplification of *ERBB2*[8–10], *CCND1*[11] or *FGFR1*[12] was common and has been previously

associated with hormone resistance but were not commonly observed to be “acquired” among those cases where we had information on the primary tumor..

The mutations in *ESR1* clustered in a small region that encodes its ligand binding domain (LBD) and were obvious candidates for mediating hormone resistance. In addition to the 7 of 22 tumors with matched normal DNA, two more mutations in the LBD were detected in the 14 samples without matched normal DNA (a total of 9/36 cases). The clinical histories of these patients reveal that they were treated with multiple lines of hormonal therapies for an average of 4.9 years (range 1–10 years) (Table 1). Of note, all 9 patients with *ESR1* mutations were treated at some point with aromatase inhibitors, drugs that reduce levels of circulating estrogens. We were able to obtain pretreatment, primary tumor samples from 2 of these 9 patients with *ESR1* mutations and the mutation was not present in either case. These primaries did harbor several other alterations that were identified in the paired metastatic sample. Among all the cases with *ESR1* mutation, 2 cases harbored concurrent *PIK3CA* mutations, 2 cases had concurrent *GATA3* mutations and 1 case had both concurrent *PIK3CA* and *GATA3* mutations. No other mutations were concurrent with *ESR1* mutation. In a separate analysis of 26 ER− tumors, no *ESR1* LBD mutation was detected (unpublished data). All *ESR1* mutations were located within the LBD/activation function-2 (AF-2) domain of the receptor and the majority occurred specifically at amino acids 537 and 538 of helix 12 (Fig. 1c).

The finding of LBD mutations in our small cohort of metastatic samples but not in several large whole genome analyses of untreated primary tumors was notable and we sought to validate this observation in another cohort of tumors. We analyzed the tumors collected from patients who enrolled in the BOLERO-2 clinical trial, which studied patients with ER+ metastatic breast cancers whose tumors had progressed on an aromatase inhibitor[13]. Most of these tumors were collected prior to any exposure to hormonal therapy (primary tumors), however a subset was collected after some exposure to hormonal therapy (metastatic tumors). Among the metastatic tumors analyzed (Foundation Medicine sequencing panel, >600x average coverage), *ESR1* mutations were observed in 11% of the cases (5/44) with only 3% (6/183) of the primary tumors mutated (Supplementary Fig. 1). Once again, mutation at Tyr537 and Asp538 of the LBD was frequently observed and occurred in patients with prolonged hormonal treatment (average of 4 years) (Table 2 and Supplementary Table 2). While there were not sufficient mutant tumors to formally analyze their ability to predict response to therapy on the BOLERO-2 clinical trial, there did not seem to be obvious differences in how mutant and wild type patients fared on the aromatase inhibitor plus placebo arm of the study. This is not surprising as all patients had already had tumor progression on an aromatase inhibitor. Given the strong correlation of LBD mutations in these two tumors sets with hormone resistant disease, we set out to characterize the functional significance of the more frequent mutations (p.Asp538Gly, p.Tyr537Ser and p.Ser463Pro) for ER activity and sensitivity to hormonal therapy.

ERα LBD mutations promote estrogen-independent receptor activation

Mutation of Tyr537 to serine was previously demonstrated to promote the ER agonist conformation and activation of its transcriptional functions[14,15]. To determine the activity of

the newly identified mutants, we introduced specific mutations by site-directed mutagenesis into hemagglutinin (HA)-tagged *ESR1* constructs. The constructs were co-transfected into breast cancer cells along with reporter plasmids carrying estrogen responsive element (ERE)-luciferase and Renilla-luciferase (pRL-TK). In ER− SKBR3, the levels of luciferase activity in the absence of estradiol (E2) were highest (60X WT levels) in cells expressing Tyr537Ser, followed by double mutant Ser463Pro/Asp538Gly (30X WT levels), and Asp538Gly (15X WT levels) (Fig. 2a). The addition of 10 nM of E2 potently induced the activity of WT receptor (5X basal WT levels) and the Ser463Pro mutant (3X basal Ser463Pro levels), while only weakly increasing the already high levels driven by the Tyr537Ser (1.4X basal Tyr537Ser level), Asp538Gly (1.5X basal Asp538Gly level), and Ser463Pro/Asp538Gly (1.6X basal Ser463Pro/Asp538Gly level) mutants. In the ER driven MCF7, these assays again revealed that the 537 and 538 mutants had very high basal activity with modest further induction by E2 (Fig. 2a). Expression of the Ser463Pro mutant induced modest activity in the absence of hormone and required E2 addition to achieve levels near those seen with the 537 or 538 mutants without hormone. We examined the activity of the mutants in 4 other cell lines (consisting of breast and endometrial models) and found in all cases Tyr537Ser and Asp538Gly could potently induce activity in the absence of hormone to near or above the levels achieved by estradiol activation of WT receptor while Ser463Pro was weakly activating (Supplementary Fig. 6a–f). These results suggest that the 537 and 538 mutations can effectively promote ER transactivation function in the absence of hormone but still bind and are responsive to ER agonists.

Given the elevated activity of the mutants on an ERE, we next asked if they could activate known ER dependent transcripts. HA-ER constructs were transfected into MCF7 cells in hormone-depleted medium and the mRNA levels of ER target genes (*GREB1, MYC, PGR, TFF1, XBP* and *CTSD*) were measured. To control for potential differences in expression of the ER constructs, the mRNA level of ER target genes was normalized to the total *ESR1* mRNA level (similar data was obtained when normalized to actin – Supplementary Fig. 4). As compared to WT ER, cells expressing Tyr537Ser, Ser463Pro/Asp538Gly and Asp538Gly mutants had significantly higher levels of *GREB1, MYC, PGR* and *TFF1* mRNA expression (Fig. 2b). To further assess if the mutants promote transcriptional functions in absence of hormone, we performed gene expression analysis of MCF7 cells transfected with the various ER mutant constructs in hormone-depleted media. In comparison to the WT, the mutants differentially regulated a total of 203 genes, of which, 92 were shared among the mutants. Hierarchical clustering of these genes showed that Tyr537Ser, Asp538Gly and Ser463Pro/Asp538Gly mutants grouped together and induced a shared gene expression pattern distinct from that of the WT (Fig. 2c). This is in agreement with the quantitative PCR and ERE-luciferase results, and taken together demonstrate that in the absence of estradiol, the Tyr537Ser and Asp538Gly mutants activate ER transcription function much more potently than WT ER.

Serine 118 (S118) is one of the major phosphorylation sites of ER[16]. Located within the AF-1 domain, S118 phosphorylation has been shown to modulate the ligand-independent activity of ER[17]. All mutants displayed elevated levels of S118 phosphorylation compared to ER WT, with Tyr537Ser and Ser463Pro/Asp538Gly showing the highest levels (Fig. 2d).

The degree of phosphorylation of the mutant receptors corresponded to the degree of luciferase activation and induction of ER target genes, further suggesting that the mutants possess higher estrogen-independent activity.

Coregulators recruited by ER can either promote (coactivators) or suppress (corepressors) the transcription of ER target genes. The binding of these coregulators specifies the response of target genes to a particular receptor-ligand complex. Among these coregulators, AIB1 plays a critical role as a coactivator for ER target gene expression[18,19]. We sought to determine the effect of LBD mutations on the interaction of ER and AIB1 by co-immunoprecipitation. In comparison to the WT, a significantly higher level of AIB1 was co-immunoprecipitated with the Asp538Gly mutant (Fig. 2e). These data further suggest that the Asp538Gly mutant promotes ER function through direct effects on ER conformation.

In the absence of ligand, ER associates with the heat shock protein 90 (Hsp90) complex, which promotes its conformational stability[20]. As the ER mutants are able to promote transcription in an estrogen-independent manner, we speculated they might be less dependent on chaperone function for their stability. To test this, MCF7 cells transfected with HA-ER WT or mutants were treated with an ATP competitive inhibitor of Hsp90, SNX2112[21], for 3 hours and the ER protein level was assessed by immunoblotting. Both Tyr537Ser and Asp538Gly were unaffected by Hsp90 inhibition while WT protein level substantially decreased in a dose dependent fashion (Fig. 2f). In further support, SNX2112 treatment in hormone deprived media demonstrated a significantly more rapid and profound depletion of WT than mutant ER (Supplementary Fig. 2). These data further suggests potential differences between the WT and mutant conformations and activities.

The higher activities of the Tyr537Ser and Asp538Gly mutant receptors suggested that they might promote hormone-independent tumor cell growth. To test this, we generated stable MCF7 cell lines in which expression of the HA-ER WT, Tyr537Ser and Asp538Gly mutants was made to be under the control of the tetracycline promoter (Supplementary Fig. 5). Tumors were established in nude mice with these MCF7 sublines in the presence of 17β-estradiol pellets surgically implanted in the mice three days before injecting the cells. The pellets were removed when the tumors reached the size of ~250 mm^3 to mimic estrogen deprivation therapy. To induce the expression of the HA-ER WT and mutants in the tumor cells, the mice were fed with water containing 0.2–0.5 mg/ml of doxycycline and 1% sucrose a week after the removal of the 17β-estradiol pellets. As shown in Figure 2g, the growth rate of all tumors was significantly reduced during the week where estrogen and doxycycline were absent, indicating their dependence on ER signaling. However induction of Tyr537Ser or Asp538Gly expression dramatically increased tumor growth (Fig. 2g). These data further confirm the sufficiency of the Tyr537Ser and Asp538Gly mutants to facilitate hormone independent ER function.

Residual activity of Y537S and D538G ER mutants after ER inhibition

Mutations in 537 and 538 appeared to strongly promote various ER activities in the absence of ligand. One of the primary modes of treatment of ER+ breast cancer is estrogen deprivation. Our data suggest that Asp538Gly and Tyr537Ser mutant forms of ER can adopt an agonist confirmation irrespective of hormone availability. However, drugs directly

targeting ER such as tamoxifen or fulvestrant may still be effective against the mutant forms of ER. To test if LBD mutants might resist ER targeted therapies, we examined the effect of 4-hydroxytamoxifen (4-OHT) or fulvestrant over a range of doses in transfected SKBr3 cells. Given the mixed agonist/antagonist effects of 4-OHT, a low dose of E2 (1 nM) was included to focus on the antagonist property in these experiments[22]. Consistent with previous reports, 4-OHT potently inhibits the activity of the Tyr537Ser mutant[23]. The drug can also potently antagonize the Asp538Gly mutant with inhibition of ~70% activity of Asp538Gly and Tyr537Ser using 10 nM 4OHT (Fig. 3a). However, also notable is the amount of residual activity that remains in these cells. In order to block ER activity to near the levels observed with the vector transfected cells, significantly higher doses of drug are required. We examined this phenomenon across a panel of cell lines and found similar results, 4-OHT can potently antagonize the Tyr537Ser and Asp538Gly mutants, but at lower doses (e.g. 1–10 nM) there is higher residual activity than for WT or vector transfected cells (Supplementary Fig. 6 and 7). Bazedoxifene, which is a third generation SERM, exhibited similar effects as 4-OHT (data not shown). The pure antiestrogen, fulvestrant, also displayed a similar phenomenon as 4-OHT (Fig. 3b) with low doses (1–5nM) decreasing activity of 537 and 538 mutants, but significantly higher doses (50–100nM) needed to bring levels closer to those of WT ER. As the doses at which potent ER inhibition is achieved in the mutant expressing models may exceed steady state, intratumoral levels achieved in patients, the data raise the possibility that more potent or selective ER antagonists will be required to effectively inhibit the 537 and 538 ER mutants.

Molecular dynamics simulation of coactivator-bound ER D538G reveals a mechanistic hypothesis

The crystal structures of agonist bound WT ER and Tyr537Ser mutated ER have been previously determined[14,24]. To directly examine the possible effects of the p.Asp538Gly mutation on ER conformation, we performed molecular dynamics (MD) simulations for ER WT, Tyr537Ser, and Asp538Gly structures, each in absence of ligand and with a coactivator (TIF2) bound. The stability of each ER variant in an agonist conformation was then assessed by the root mean squared difference (RMSD) between the starting agonist conformation and the final conformation after 10-ns MD simulations.

Among the 3 coactivator-bound ER variants, ER WT showed the largest difference from the starting agonist conformation (Fig. 4a), in which the cofactor recruiting helix 12 (H12, which starts with residue 538) drifted away from the rest of ER structure (including helix 3, H3) by 2.1 Å in RMSD. In clear contrast with ER WT was ER Tyr537Ser, in which H12 stayed close to the starting agonist conformation (Fig. 4b), with H12 RMSD being 1.2 Å. A hydrogen bond between side chains of Ser537 and Asp351 was observed in the 10-ns MD structure of ER Tyr537Ser (Fig. 4b insert). This hydrogen bond was found to be stable throughout the MD simulation and existed for 99.8% of the last 1 ns (Fig. 4d). In other studies, it was introduced to facilitate structural determination of ER–agonist complexes and observed in corresponding X-ray crystal structures[14].

In the case of ER Asp538Gly, the starting residue 538 of H12 shifted towards H3 by 3.5 Å (Fig. 4c). Remarkably, hydrogen bonds were formed between the backbone of Gly538 (a

nitrogen atom as donor) and the side chain of Asp351 (2 oxygen atoms as acceptors). For simplicity, a single distance between the hydrogen and its closer acceptor at Asp351 was measured for each snapshot of the simulations. Judging from a standard 2.4-Å cutoff in hydrogen-to-acceptor distance, Gly538–Asp351 hydrogen bond(s) was stable during the simulation and existed for 94.3% of the last 1 ns (Fig. 4d). In contrast, no hydrogen bond was found between residue Gly538 and Asp351 in ER WT either in the crystal structure or during the simulation. Even though the rest of H12 drifted away from H3 by 2.8 Å, we speculate that the hydrogen bonds can keep H12 from moving away from its agonist conformation significantly further. Judging from the slightly longer hydrogen-to-acceptor distances and lower existence percentage in the last 1 ns of simulations, the Gly538–Asp351 hydrogen bond(s) in ER Asp538Gly appeared weaker than Tyr537Ser–Asp351. The Gly538–Asp351 hydrogen bond(s) was very likely enabled by the substituent glycine, which is the smallest and the most flexible among all amino acids and can adopt backbone conformations inaccessible to other amino acids. Indeed, this hypothesis was supported by the unique Π angle (the dihedral around N–C_α bond) at residue 538 modeled for ER Asp538Gly (−125° compared to around −49° for ER WT and Tyr537Ser, crystallized or MD-simulated). This hypothesis was further supported by a functional experiment in which mutating residue 538 to an alanine (uncharged and small like glycine) had no effect on ER transactivation function (Supplementary Fig. 3). Taken together, the conformational choices of ER WT, Tyr537Ser, and Asp538Gly modeled correlate with their basal activity levels and provide a mechanistic explanation for the newly discovered activating mutation Asp538Gly.

Discussion

In this report, we identify for the first time recurrent mutations in the LBD of *ESR1* in approximately 20% of metastatic ER+ breast cancer. The mutations occur in a population of patients with hormone refractory disease. The biochemical and structural data demonstrate that these mutations promote the agonist conformation of ER in the absence of ligand and likely represent one of the major causes of acquired resistance to estrogen depletion therapies such as aromatase inhibitors. The mutants appear to retain some sensitivity to drugs directly targeting the receptor suggesting potential pharmacologic strategies for these patients.

The first description of a natural LBD mutation of *ESR1* came from a patient with metastatic breast cancer in 1997[15]. Subsequent studies have interrogated exomes and genomes of primary breast cancer and failed to identify similar lesions causing many to question if the initial finding was merely an outlier[7]. In our study of metastatic breast cancer samples, we identified 9/36 tumors with mutations in the LBD of ERα. Independently, analysis of ER+ metastatic breast cancers from the BOLERO-2 trial also identified 5/44 patients with *ESR1* LBD mutations. In many regards these two studies were highly comparable with alterations in the same amino acids, lack of alterations in other domains of the protein, and mutations found in patients with prolonged prior exposure to hormonal therapy. There are two obvious differences between these two metastatic tumor cohorts and the primary tumors that previously found few to no *ESR1* mutations. First, analyzing metastatic tumors as opposed to primary tumors enforced a selection bias for more aggressive and lethal tumors. Second, in our population, patients with *ESR1* mutations were exposed to an average of 5 years of

prior hormonal therapy. Our selection of this population was imposed to facilitate understanding of a specific and understudied clinical entity, patients with acquired resistance to hormonal therapy.

In our analysis of frequently mutated oncogenes and tumor suppressors, *ESR1* mutations stood out as a common and plausible event that could contribute to resistance. We found that the mutations in both Tyr537 and Asp538 strongly promoted ER signaling in absence of ligand. This was observed biochemically as increased phosphorylation on S118, increased association with AIB1, and diminished sensitivity to HSP90 inhibitors. Functionally, the mutations in vitro promoted the expression of classical ER target genes in the absence of hormone. Moreover, expression of the Tyr537Ser and Asp538Gly mutations was sufficient to render a hormone-sensitive tumor model, MCF-7, resistant to estrogen deprivation in vivo. Interestingly, the Ser463Pro mutant was also observed in 3 patients and in all cases co-occurred with mutation in Tyr537 or Asp538. Expression of the Ser463Pro mutant was associated with a rather modest induction in ER activity (ER target gene expression) in absence of hormone, but not to near the levels seen with the Tyr537Ser or Asp538Gly mutants. Expression of this mutant together with Asp538Gly did induce activity above the level seen with Asp538Gly alone. Given the location of this residue near the dimerization interface of ER, it will be of interest to study whether the mutation alters ER dimer formation and what complementary roles it might play with mutations in Tyr537Ser and Asp538Gly in mediating hormone resistance.

Computer modeling of the structural effects of p.Tyr537Ser and p.Asp538Gly mutations helped to decipher the molecular mechanisms responsible for the hormone-independent activation of the mutants. MD stimulations of Tyr537Ser and Asp538Gly bound to TIF2 (coactivator) revealed that that both mutants favor the formation of the agonist conformation of ER (Fig. 4). Provocatively, hydrogen bonds were detected between Gly538/Ser537 and Asp351 (on H3), which existed for 94.3% and 99.8% of the last 1 ns of stimulation respectively. The latter bond formation is validated in the crystal structure of Tyr537Ser and associated with the constitutive activity of the mutant[14]. The newly discovered hydrogen bond involving Gly538 is likely caused by altered backbone conformations inaccessible to all amino acids except glycine, which is supported by the fact that Asp538Ala was non-activating. Furthermore, these stimulations agree with the activity levels of the mutants, suggesting that these hydrogen bonds stabilize the agonist conformation, especially for the co-activator recruiting helix 12 and its surroundings, and may contribute to the elevated activity of the mutants. They do not however show obvious impact on the ligand binding pocket that might hinder ER antagonists from binding. Indeed, in vitro ligand binding assays confirmed the ability of mutant LBDs to bind estradiol (data not shown). Rather, the effects on helix 12 are likely to influence coactivator/corepressor binding.

While the mutant ER isoforms were not effectively inhibited by hormone withdrawal, they could be partially inhibited by direct antagonists of the receptor like tamoxifen or fulvestrant. These findings validate previously observed data on the effect of tamoxifen on Tyr537Ser activity[23]. However, the ability of these drugs to inhibit the mutants is somewhat impaired. When we examined the effect of different doses of these compounds on mutant expressing cells, at the lower doses, significant residual activity was observed and this may

be sufficient to confer drug resistance. Moreover, expression of the mutants was observed to raise the dose of tamoxifen needed to inhibit MCF7 cell growth in vitro (data not shown). By way of anecdote, one of 9 patients in the MSKCC set did receive treatment with direct ER antagonists (tamoxifen followed by fulvestrant) after detection of this mutation and had no tumor response to either.

That, higher doses of fulvestrant or tamoxifen in vitro were able to fully antagonize mutant ER signaling is nonetheless notable. The suggestion from these data and the structural modeling is that more potent or specific antagonists of the mutant forms may be effective at blocking ER signaling and benefit patients where hormonal therapies can have a very high therapeutic index. As next generation SERMs and SERDs are in current development, analysis of their effects on the activity and stability of ER mutants is now a pressing need given the apparent prevalence of these lesions in patients with metastatic disease. Going further, the fact that these lesions are clearly more prevalent in metastatic disease suggests a possible causal role in this process. Given the widespread use of hormone antagonists as adjuvants to prevent metastatic recurrence, it will be important to determine if the mutations may be implicated in such recurrences and then whether newer SERMs/SERDs that more potently block mutant function can be curative when given as adjuvants.

Methods

Reagents

4–Hydroxytamoxifen (4-OHT) and 17β-estradiol (E2) were from Sigma-Aldrich (St Louis, MO). Fulvestrant (ICI 182780) was purchased from Selleck Chemicals, while bazedoxifene acetate (BZA) was from Toronto Research Chemical Inc (ON, Canada). SNX2112 was from Pfizer (New York, NY). All the drugs were dissolved in ethanol except for BZA and SNX2112, which was reconstituted in DMSO. Phospho-Serine 118 Estrogen receptor-α (Cat. No: 11072), hemagglutinin (HA)-tag (Cat. No: 2367/ Clone: 6E2), AIB1 (Cat. No: 611105/ Clone: 34/AIB-1) and anti-β-Actin (Cat. No: 5441/ Clone: AC-15) antibodies were purchased from Signalway Antibody, Cell Signaling Technology, BD Transduction Laboratories and Sigma respectively. GFP-trap®_A kit was from Chromotek (Germany). pcDNA 3.1 (+), pCL-Ampho and pVSVG vectors were gifts from Dr. Ping Chi (MSKCC) and pSIN-TREtight-IRES-Cherry vector was a kind gift from Dr Scott Lowe (MSKCC). pRL-TK Renilla Luciferase plasmid was from Promega, 3x-ERE-TATA-Luciferase reporter and pEGFP-C1-ERα were from Addgene, (Addgene plasmid 11354 and 28230, deposited by Donald McDonnell and Michael Mancini respectively).

Cell Culture

All cell lines were maintained at 37°C and 5% CO_2 in humidified atmosphere. SKBR-3 MCF7, ZR-75-1, MDA-MB-361, MDA-MB-231 cell lines were obtained from American Type Culture Collection, while MCF Tet-On® was from Clontech. Ishikawa cell line was obtained from Dr. Jorge S. Reis-Filho's lab. SKBr-3, MCF7, and MDA-MB-361 were grown in DMEM-F12, ZR-75-1 and MDA-MB-231 in RPMI and Ishikawa in DMEM, supplemented with 5% heat inactivated fetal bovine serum (FBS), 100 ug/ml penicillin, 100 mg/ml streptomycin, and 4mM glutamine. MCF Tet-On® cells were grown in similar

medium except for the replacement of the fetal bovine serum with 10% Tet System Approved FBS from Clontech. All cell lines were tested negative for mycoplasma.

Transfection

Cells were either transfected with Lipofectamine 2000 (Invitrogen) or X-tremeGENE (Roche) according to the manufacturer's protocol. For experiments involving estrogen induction, cells were transfected in phenol red-free DMEM-F12 containing 10% charcoal-stripped FBS (hormone-depleted medium) (Invitrogen) and E2 was added 24 hours post-transfection.

Cloning and Mutagenesis

An HA tag was inserted onto the 5′ end of ERα by PCR-amplifying it from pEGFP-C1-ERα using primers as stated in Supplementary Table 4. This HA-ERα fragment was cloned into pcDNA3.1 (+) using ApaI and BamHI restriction sites and into pSIN-TREtight-IRES-Cherry using BamHI and ApaI restriction sites. Point mutations were introduced into pEGFP-C1-ERα, pcDNA-HA-ERα and pSIN-TREtight-HA-ERα using the QuikChange II XL Site-Directed Mutagenesis Kit (Stratagene) as indicated in the manufacturer's instructions.

Clinical samples (MSKCC set)

Patients with breast cancer and either recurrence of disease after receiving adjuvant therapy or WHO-defined progression of metastatic disease on therapy were prospectively enrolled on an IRB approved tissue collection protocol from February 2007 through January 2013. Informed consent was obtained from all patients. All patients underwent biopsy of at least a single site to document progressive disease. Mutational analysis of the metastatic biopsy was performed on fresh frozen specimens. Formalin fixed paraffin embedded (FFPE) blocks of the pretreatment primary tumor was obtained where possible for comparison. The presence of tumor, in both frozen samples and FFPE tissue sections, was confirmed by the study pathologist. Extraction of genomic DNA was performed using QuickGeneTM DNA tissue kit (Fujifilm). A minimum of 5mg of fresh frozen tumor was suspended in 360 μl of tissue lysis buffer (MDT) plus 40 μl of proteinase K and incubated for 48 hours at 55°C. Lysis buffer LDT (360 μl) was then added and samples were incubated at 70°C for 30 minutes. Samples were then washed with ethanol 100% and wash buffer. Elution was in 50 μl of EDTA buffer. Quantification of DNA by Nanodrop® Fluorospectrometer showed an average yield of 20 μg (Picogreen avg yield 250 ng). A prespecified effect size was not estimated in our discovery efforts using next generation sequencing to characterize hormone refractory breast cancers.

IMPACT Next Generation Sequencing and Analysis

Extracted genomic DNA from the MSKCC clinical samples underwent next-generation sequencing using an Illumina Hiseq 2000 and analysis using our custom IMPACT assay (Integrated Mutation Profiling of Actionable Cancer Targets). The IMPACT assay uses specially designed target-specific probes to capture all protein-coding exons of 230 genes of interest for hybrid selection (Agilent SureSelect or Nimblegen SeqCap) as previously

described[25]. This list included commonly implicated oncogenes, tumor suppressor genes, and components of pathways deemed actionable by current targeted therapies (Supplementary Table 3 for complete target list). In addition to the exons of 230 cancer genes, we designed probes to target >1000 common SNP sites across the genome. For each sample, we examine all sites that are homozygous and calculate the average minor allele frequency across these sites. Tumors for which the average minor allele frequency at homozygous sites is >2% are removed, as this suggests the presence of contaminating DNA from another individual. By monitoring this closely and removing samples harboring evidence of contamination, we can increase our confidence that variants with low allele frequency are bona fide mutations and not false positive artifacts.

Two protocols were followed during the course of the study. For 8 samples (4 tumor/normal pairs), barcoded sequence libraries (Illumina TruSeq) were prepared using 500 ng of input tumor or matched normal DNA according to the manufacturer's instructions. Libraries were pooled at equimolar concentrations (100 ng per tumor library and 50 ng per normal library) for a single exon capture reaction (Agilent SureSelect) as previously described[26]. For the remaining samples, barcoded sequence libraries were prepared using 250 ng of input DNA using a hybrid protocol based on the NEBNext DNA Library Prep Kit (New England Biolabs). Manufacturer's instructions were followed with two substitutions: we used NEXTflex barcoded adapters (Bio Scientific) and HiFi DNA polymerase (Kapa Biosystems). Libraries were pooled at 100 ng per tumor library and 50 ng per normal library for a single exon capture reaction (Nimblegen SeqCap). To prevent off-target hybridization in all capture reactions, we spiked in a pool of blocker oligonucleotides complementary to the full sequences of all barcoded adaptors (to a final total concentration of 10 μM). Hybridized DNA was sequenced on an Illumina HiSeq 2000 to generate paired-end 75-bp reads.

Data were demultiplexed using CASAVA, and reads were aligned to the reference human genome (hg19) using the Burrows-Wheeler Alignment tool[27]. Local realignment and quality score recalibration were performed using the Genome Analysis Toolkit (GATK) according to GATK best practices[28]. We achieved mean exon sequence coverage of 512X (628x for all tumor samples and 418X for all normal samples). Deep sequencing ensured sensitivity for detecting mutations in multiclonal and stroma-admixed samples and enabled accurate determination of mutation allele frequencies.

Sequence data were analyzed to identify three classes of somatic alterations: single-nucleotide variants, small insertions/deletions (indels), and copy number alterations. Single-nucleotide variants were called using muTect (Cibulskis et al., manuscript in preparation) and retained if the variant allele frequency in the tumor was >5 times that in the matched normal. Indels were called using the SomaticIndelDetector tool in GATK. All candidate mutations and indels were reviewed manually using the Integrative Genomics Viewer[29]. The mean sequence coverage was calculated using the DepthOfCoverage tool in GATK and was used to compute copy number as described previously[6].

Clinical Samples (BOLERO-2 sample set)

The study design for BOLERO-2 has been described previously[13]. Archival tissue samples with sufficient tumor content (10, 4-μm slides/patient) were identified and analyzed by next generation sequencing.

Foundation Medicine Next Generation Sequencing and analysis (BOLERO-2 set)

Next generation sequencing and analysis by Foundation Medicine was performed as described previously[30]. DNA sequencing was performed for 3230 exons of 182 cancer genes on indexed, adaptor ligated, hybridization-captured (Agilent SureSelect custom kit) libraries using DNA isolated from 272 FFPE tumors along with matched normal DNA from WBCs. A total of 227 samples (183 primary + 44 metastatic) with coverage >250X and average coverage of 602 ± 202X were included in the final analysis.

Retroviral infection and generation of stable cell lines

293CT packaging cells were plated at 2.5 X 10^7 cells/10-cm-diameter tissue culture dishes and transfected with 2.25 ug of the pSIN-TREtight retroviral vector (empty or containing HA-WT or mutant ER), 2.25 ug of pCL-Ampho and 0.5 ug of pVSVG with X-tremeGENE (Roche) according to the manufacturer's protocol. The conditioned medium containing recombinant retroviruses was collected and filtered through 0.45 μm-pore-size non-pyrogenic filters (Millipore). Samples of these supernatants were applied immediately to MCF Tet-On® cells, which had been plated 18 hours before infection at a density of 4 x 10^6 cells/10-cm-diameter tissue culture dishes. Polybrene (Sigma, St. Louis, MO, USA) was added to a final concentration of 8 μg/ml, and the supernatants were incubated with the cells for 12 hours. After infection, the cells were placed in fresh growth medium and cultured as usual. Selections with 500 μg/ml of hygromycin were initiated 72 hours after infection. After 14 days of selection, hygromycin concentration was lowered to 100 μg/ml and the cells were cultured as usual.

Animal studies

6–8 week old nu/nu athymic BALB/c female mice were obtained from Harlan Laboratories, Inc. and maintained in pressurized ventilated caging. All studies were performed in compliance with institutional guidelines under an IACUC approved protocol (MSKCC#12-10-016). MCF7 inducible HA-ER xenograft tumors were established in nude mice by subcutaneously implanting 0.72 mg sustained release 17β-estradiol pellets with a 10g trocar into one flank followed by injecting 1×10^7 cells suspended 1:1 (volume) with reconstituted basement membrane (Matrigel, Collaborative Research) on the opposite side 3 days afterwards. The 17β-estradiol pellets were removed from the mice when tumors reached a size of ~250 mm^3 and then fed with water containing 0.2/0.5 mg/ml of doxycycline (0.2 mg/ml for WT and 0.5 mg/ml for vector control, Y537S and D538G respectively) and 0.1% sucrose for induction of ER expression, 7 days after pellet removal. Tumor dimensions were measured with vernier calipers and tumor volumes calculated ($\pi/6 \times$ larger diameter $\times$ (smaller diameter)^2). In this study, no blinding of investigator or randomization of animals was done. Based upon our previous work measuring the

variability in size and growth of MCF7 xenografts, we estimated 10 mice/group would allow us to detect tumor size differences of >200mm^3.

Coimmunoprecipitation

Coimmunoprecipitation (coIP) was performed with the GFP-Trap®_A kit according to the manufacturer's protocol. In brief, cell pellets were resuspended with the CoIP lysis buffer (10mM Tris/Cl, pH7.5, 150mM NaCl, 0.5mM EDTA, 0.5% NP40, 1X protease and phosphatase inhibitors (Pierce)). Cells were lysed by pipetting the pellet up and down every 10 minutes for a total of 30 minutes while on ice. Lysates were cleared by spinning them at 20,000 g for 10 minutes. For the coIP, 1 mg of lysate was used for each sample with a 100 ul of equilibrated GFP®-Trap_A beads and incubated on a rotator overnight at 4°C. The beads were then washed twice with ice cold wash buffer, resuspended with 2X LDS sample buffer (Invitrogen) and boiled for 10 minutes at 70°C before loading onto the SDS-PAGE gels.

Immunoblotting

Cells were washed once with cold PBS and scraped off the plate with a rubber policeman. The cell suspension was briefly centrifuged to pellet down the cells, PBS was removed and the cell pellet was stored at −80°C until lysis. For cell lysis, the pellets were resuspended in a non-denaturing lysis buffer (Cell Signaling), supplemented with protease and phosphatase inhibitors (Pierce) and sonicated briefly for 30 seconds. Lysates were cleared by centrifugation at 14,000 g for 10 minutes and protein concentrations of samples were determined using the BCA kit (Pierce), which measures the reduction of Cu^{2+} to Cu^{1+} by protein in an alkaline medium. For each sample, thirty micrograms of protein lysate was loaded onto 4–12% SDS-PAGE minigels (Invitrogen) for electrophoresis and immunoblotting.

Luciferase Assays

Cells were plated at a density of 0.1×10^6 per well of 24 well plates one day prior to transfection. Cells were transfected with 100 ng (per well) of HA-ERα wild type or mutants, 250 ng (per well) of 3x-ERE-TATA-Luciferase reporter and 50 ng (per well) of pRL-TK Renilla Luciferase plasmid, using Lipofectamine 2000 (Invitrogen). The cells were treated either with E2, 4-OHT or ICI a day after transfection for 24 hours and luciferase activities were determined using the Dual-Luciferase® Reporter Assay System (Promega) according to manufacturer's instructions. Luciferase bioluminescence measurements were performed with the Veritas™ Microplate Luminometer (Promega). All experiments were conducted in triplicate and the Firefly luciferase activity was normalized with the Renilla luciferase activity of each sample.

Quantitative RT-PCR

RNA was extracted from cells 48h post-transfection using the RNeasy Mini Kit (Qiagen) according to the manufacturer's protocol. cDNA was synthesized from 2 ug of RNA of each sample using the SuperScript® First-Strand Synthesis System for RT-PCR (Invitrogen) as per manufacturer's protocol. Synthesized cDNA was diluted with one volume of DEPC-treated water and 2 ul of the mixture was mixed with TaqMan® PCR Master Mix (Applied

Biosystems) and primers. The relative quantification of each mRNA was performed using the comparative Ct method with a ViiA™ 7 Real-Time PCR system (Applied Biosystems)[31]. Samples were run in triplicate and normalized to the levels of *ESR1* for each reaction.

Microarray

RNA was extracted from MCF7 cells transfected with GFP-ERα WT and mutants using TRIzol reagent and analyzed with the HumanHT-12 v4 Expression BeadChip (Illumina). Statistical analysis of differences between each group was evaluated using standard ANOVA test. Data were analyzed using Partek Genomics Suite.

Molecular dynamics simulations

The crystal structures of TIF2-bound ER WT and Tyr537Ser were taken from the Protein Data Bank[6] (accession codes 1GWQ and 3Q95 respectively). Their corresponding agonist ligands were removed. A few terminal residues on ER or TIF2 were also removed so that the two structures share the same segments. The structure of TIF-2 bound ER Asp538Gly was first built by removing the side chain atoms at residue 538. For all these 3 structures, missing atoms were placed with CHARMM22[32]-parameterized geometries and then minimized with the rest harmonically constrained, using the molecular modeling program CHARMM[33]. The minimization was done with a distant-dependent dielectric constant to approximate solvation effects. No distance cutoff for non-bonded interactions was used.

The resulting structures were used as starting points for explicit-solvent molecular dynamics simulation. Each was first placed in a water box whose boundaries were at least 15 Å away from the nearest ER or TIF2 atoms. Sodium and chloride ions were also added to reach a physiological concentration (0.145 M) and total charge neutrality. The two steps above were performed with the program VMD[34]. Each system of TIF2-bound ER (WT, Tyr537Ser, or Asp538Gly), water molecules, and ions was minimized for 5000 steps and then run for a 10-ns molecular dynamics stimulation using the program NAMD[34]. A constant temperature (300 K) and pressure (1 atm, with Nosé-Hoover Langevin piston method) were used for the MD simulations. Force field parameters were adopted from CHARMM22. Electrostatic interactions were treated with a particle mesh Ewald (PME) method (1-Å grid spacing and 14-Å distance cutoff). The dynamics were run with a 2-fs time step and the list of nonbonded interactions updated every 10 steps.

Statistics

All reported values represent the average of triplicates. Statistical analysis of differences between samples were evaluated using standard 2-tailed Student t-test and $P < 0.05$. Analysis was conducted using Prism v6.0c (GraphPad Software).

Supplementary Material

Refer to Web version on PubMed Central for supplementary material.

Acknowledgments

We would like to thank Neal Rosen and Charles Sawyers for their insights and critical reading of the manuscript. S.C is funded by the Damon Runyon Cancer Research Foundation and a Louis V. Gerstner Jr. Young Investigator Award. Individual support for this study was also provided by Julie Laub (to C.H.). Molecular dynamics simulations were performed using computational resources awarded to Y.S. by the Argonne Leadership Computing Facility at Argonne National Laboratory, which is supported by the Office of Science of the U.S. Department of Energy under contract DE-AC02-06CH11357. Y.S. is partially funded by the Toyota Technological Institute at Chicago.

References

1. Effects of chemotherapy and hormonal therapy for early breast cancer on recurrence and 15-year survival: an overview of the randomised trials. Lancet. 2005; 365:1687–717. [PubMed: 15894097]
2. Ariazi EA, Ariazi JL, Cordera F, Jordan VC. Estrogen receptors as therapeutic targets in breast cancer. Curr Top Med Chem. 2006; 6:181–202. [PubMed: 16515478]
3. Strasser-Weippl K, Goss PE. Advances in adjuvant hormonal therapy for postmenopausal women. J Clin Oncol. 2005; 23:1751–9. [PubMed: 15755983]
4. Forbes JF, et al. Effect of anastrozole and tamoxifen as adjuvant treatment for early-stage breast cancer: 100-month analysis of the ATAC trial. Lancet Oncol. 2008; 9:45–53. [PubMed: 18083636]
5. Peng J, Sengupta S, Jordan VC. Potential of selective estrogen receptor modulators as treatments and preventives of breast cancer. Anticancer Agents Med Chem. 2009; 9:481–99. [PubMed: 19519291]
6. Wagle N, et al. High-throughput detection of actionable genomic alterations in clinical tumor samples by targeted, massively parallel sequencing. Cancer Discov. 2012; 2:82–93. [PubMed: 22585170]
7. Comprehensive molecular portraits of human breast tumours. Nature. 2012; 490:61–70. [PubMed: 23000897]
8. Gutierrez MC, et al. Molecular changes in tamoxifen-resistant breast cancer: relationship between estrogen receptor, HER-2, and p38 mitogen-activated protein kinase. J Clin Oncol. 2005; 23:2469–76. [PubMed: 15753463]
9. Lipton A, et al. Serum HER-2/neu conversion to positive at the time of disease progression in patients with breast carcinoma on hormone therapy. Cancer. 2005; 104:257–63. [PubMed: 15952182]
10. Meng S, et al. HER-2 gene amplification can be acquired as breast cancer progresses. Proc Natl Acad Sci U S A. 2004; 101:9393–8. [PubMed: 15194824]
11. Jirstrom K, et al. Adverse effect of adjuvant tamoxifen in premenopausal breast cancer with cyclin D1 gene amplification. Cancer Res. 2005; 65:8009–16. [PubMed: 16140974]
12. Turner N, et al. FGFR1 amplification drives endocrine therapy resistance and is a therapeutic target in breast cancer. Cancer Res. 2010; 70:2085–94. [PubMed: 20179196]
13. Baselga J, et al. Everolimus in postmenopausal hormone-receptor-positive advanced breast cancer. N Engl J Med. 2012; 366:520–9. [PubMed: 22149876]
14. Nettles KW, et al. NFkappaB selectivity of estrogen receptor ligands revealed by comparative crystallographic analyses. Nat Chem Biol. 2008; 4:241–7. [PubMed: 18344977]
15. Zhang QX, Borg A, Wolf DM, Oesterreich S, Fuqua SA. An estrogen receptor mutant with strong hormone-independent activity from a metastatic breast cancer. Cancer Res. 1997; 57:1244–9. [PubMed: 9102207]
16. Kato S, et al. Activation of the estrogen receptor through phosphorylation by mitogen-activated protein kinase. Science. 1995; 270:1491–4. [PubMed: 7491495]
17. Le Goff P, Montano MM, Schodin DJ, Katzenellenbogen BS. Phosphorylation of the human estrogen receptor. Identification of hormone-regulated sites and examination of their influence on transcriptional activity. J Biol Chem. 1994; 269:4458–66. [PubMed: 8308015]
18. Anzick SL, et al. AIB1, a steroid receptor coactivator amplified in breast and ovarian cancer. Science. 1997; 277:965–8. [PubMed: 9252329]

19. Azorsa DO, Cunliffe HE, Meltzer PS. Association of steroid receptor coactivator AIB1 with estrogen receptor-alpha in breast cancer cells. Breast Cancer Res Treat. 2001; 70:89–101. [PubMed: 11768608]
20. Fan M, Park A, Nephew KP. CHIP (carboxyl terminus of Hsc70-interacting protein) promotes basal and geldanamycin-induced degradation of estrogen receptor-alpha. Mol Endocrinol. 2005; 19:2901–14. [PubMed: 16037132]
21. Chandarlapaty S, et al. SNX2112, a synthetic heat shock protein 90 inhibitor, has potent antitumor activity against HER kinase-dependent cancers. Clin Cancer Res. 2008; 14:240–8. [PubMed: 18172276]
22. Shang Y, Brown M. Molecular determinants for the tissue specificity of SERMs. Science. 2002; 295:2465–8. [PubMed: 11923541]
23. Weis KE, Ekena K, Thomas JA, Lazennec G, Katzenellenbogen BS. Constitutively active human estrogen receptors containing amino acid substitutions for tyrosine 537 in the receptor protein. Mol Endocrinol. 1996; 10:1388–98. [PubMed: 8923465]
24. Brzozowski AM, et al. Molecular basis of agonism and antagonism in the oestrogen receptor. Nature. 1997; 389:753–8. [PubMed: 9338790]
25. Won H, SS. Detecting Somatic Genetic Alterations in Tumor Specimens by Exon Capture and Massively Parallel Sequencing. Journal of Visualized Experiments. 2013
26. Li H, et al. The Sequence Alignment/Map format and SAMtools. Bioinformatics. 2009; 25:2078–9. [PubMed: 19505943]
27. Li H, Durbin R. Fast and accurate short read alignment with Burrows-Wheeler transform. Bioinformatics. 2009; 25:1754–60. [PubMed: 19451168]
28. DePristo MA, et al. A framework for variation discovery and genotyping using next-generation DNA sequencing data. Nat Genet. 2011; 43:491–8. [PubMed: 21478889]
29. Robinson JT, et al. Integrative genomics viewer. Nat Biotechnol. 2011; 29:24–6. [PubMed: 21221095]
30. Lipson D, et al. Identification of new ALK and RET gene fusions from colorectal and lung cancer biopsies. Nat Med. 2012; 18:382–4. [PubMed: 22327622]
31. Chandarlapaty S, et al. AKT inhibition relieves feedback suppression of receptor tyrosine kinase expression and activity. Cancer Cell. 2011; 19:58–71. [PubMed: 21215704]
32. MacKerell AD, Bashford JD, Dunbrack M, Evanseck RL Jr, Field JD, Fischer MJ, Gao S, Guo J, Ha H, Joseph-McCarthy S, Kuchnir DL, Kuczera K, Lau FTK, Mattos C, Michnick S, Ngo T, Nguyen DT, Prodhom B, Reiher WE III, Roux B, Schlenkrich M, Smith JC, Stote R, Straub J, Watanabe M, Wiorkiewicz-Kuczera J, Yin D, Karplus M. All-Atom Empirical Potential for Molecular Modeling and Dynamics Studies of Proteins. J Phys Chem B. 1998; 102:3586–3616. [PubMed: 24889800]
33. Brooks BR, et al. CHARMM: the biomolecular simulation program. J Comput Chem. 2009; 30:1545–614. [PubMed: 19444816]
34. Phillips JC, et al. Scalable molecular dynamics with NAMD. J Comput Chem. 2005; 26:1781–802. [PubMed: 16222654]

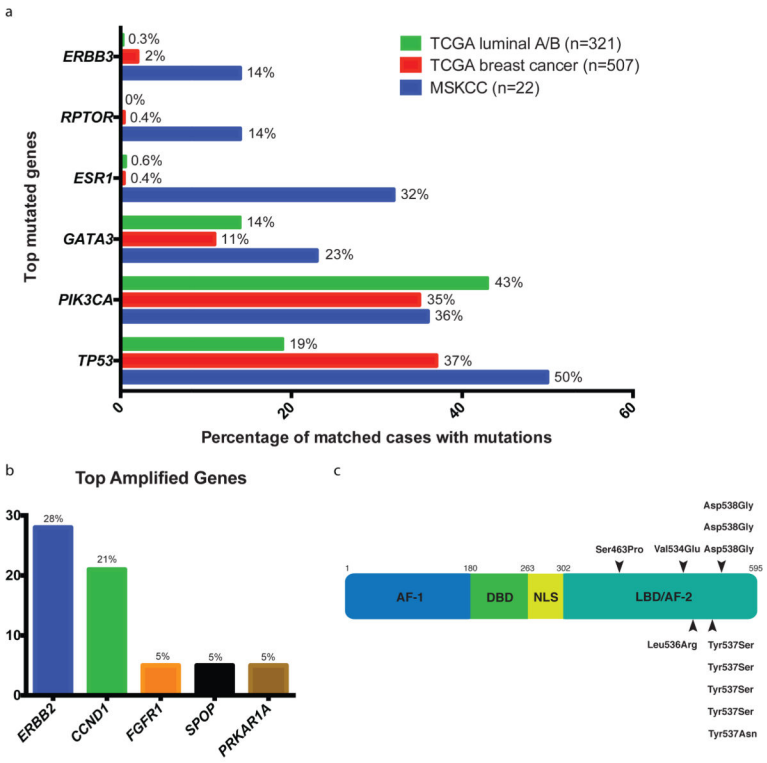

Figure 1. *ESR1* mutations in ER+ metastatic breast cancers

a. Percentage of matched cases with gene mutations detected in our patient samples (MSKCC) were compared to those of The Cancer Genome Atlas (TCGA) invasive breast cancer and luminal A/B cases. Only genes found mutated in 3 or more cases are shown. **b.** Top amplified genes detected in the patient samples. Genes were considered amplified when the ratio of their copy number in tumor to normal is greater than 2 **c.** Diagram of ER domains with the location of the identified mutations. AF-1: Activation Function-1; DBD: DNA binding domain; NLS: Nuclear localizing signal; LBD: Ligand binding domain; AF-2: Activation function-2.

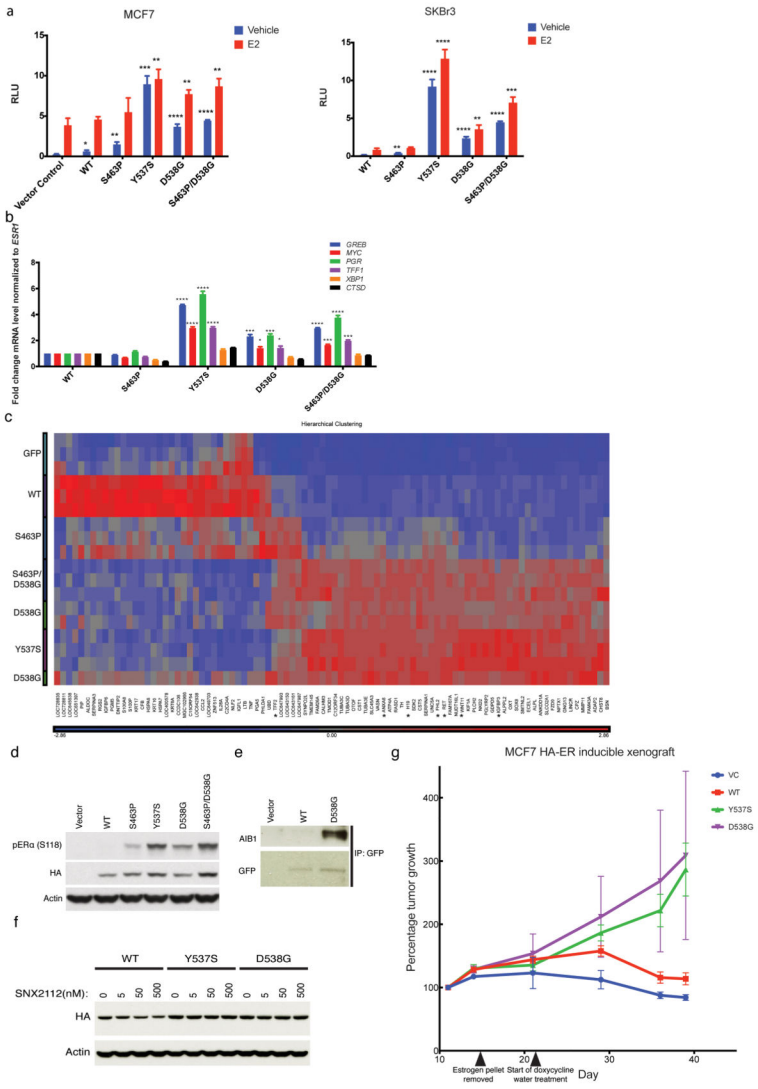

Figure 2. ERα LBD mutants demonstrate elevated activity in absence of hormone

a. SKBR3 and MCF7 cells were transfected with empty vector, HA-ERα wild type (WT) or mutants, ERE-luciferase and Renilla luciferase reporter constructs in hormone-depleted medium with 10 nM of E2 added for 24 hours where indicated. Relative light units (RLU) were calculated as the ratio of Firefly luciferase over Renilla luciferase activity. Graph was plotted with the mean ± SD of triplicate biological replicates. *, $P < 0.05$; **, $P < 0.01$; ***, $P < 0.001$; ****, $P < 0.0001$. **b.** MCF7 cells were transfected with HA-ERα wild type (WT) or mutants in hormone-depleted medium and harvested 48 hours post-transfection. The mRNA level of ERα target genes were quantified by qRT-PCR using gene-specific primers. Bars represent mean ± SD of triplicate technical replicates normalized to *ESR1* expression. *, $P < 0.05$; ***, $P < 0.001$; ****, $P < 0.0001$. The data shown is a representative of two biological replicates. **c.** Gene expression microarray was performed using RNA derived from MCF7 cells transfected with empty vector, GFP-ERα WT or mutants in hormone-depleted medium for 48 hours. A total of 92 genes were commonly up or down-regulated by the ERα mutants and they were hierarchically clustered to generate a heat map. Selected

genes previously well established as estrogen responsive genes were marked with *. **d.** Lysates of MCF7 cells transfected with empty vector, HA-ERα WT or mutants in hormone-depleted medium for 48 hours, were immunoblotted with phospho-Serine 118 of ERα, HA and actin antibodies. The immunoblots shown are a representative of experiments repeated at least three times. **e.** Lysates generated from MCF7 transfected with empty vector GFP-ERα WT, or D538G were immunoprecipitated with GFP-Trap beads and immunoblotted with AIB1 and GFP antibodies. The immunoblots shown are a representative of experiments repeated three times. **f.** MCF7 cells transfected with HA-ERα WT or mutants were treated with SNX2112 at various doses for 3 hours before harvest. Lysates were then immunoblotted with HA and actin antibodies. The immunoblots shown are a representative of experiments repeated three times. **g.** Mice bearing MCF7 inducible vector control (VC), HA-ER WT or Tyr537Ser or Asp538Gly tumors had their 17β-estradiol pellets removed when the tumors reached an approximate volume of 250 mm^3 and then fed with water containing 0.2–0.5 mg/ml of doxycycline a week after for the induction of ER WT and mutant expression. The result was presented as percentage tumor growth by normalizing to the first mean tumor volume measured for each group ± SEM (n = 10 mice/group).

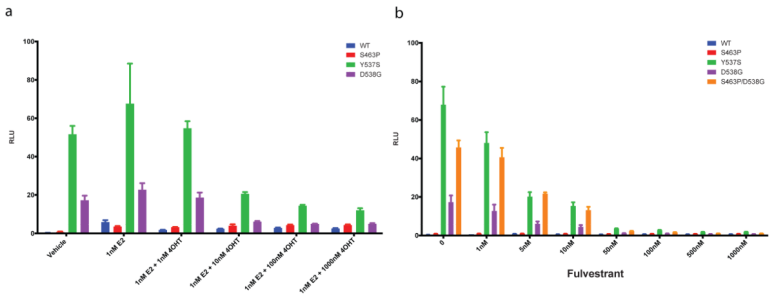

Figure 3. ER antagonists partially inhibit ER mutant transcriptional activity

SKBR3 cells were transfected with HA-ERα WT or mutants, ERE-luciferase and Renilla luciferase reporter constructs in hormone-depleted medium. The cells were then treated with either **a.** 1 nM E2 alone or in combination with 4-OHT (4-hydroxytamoxifen) and **b.** fulvestrant at the indicated doses for 24 hours before luciferase activity measurement. Relative light units (RLU) were calculated as the ratio of Firefly luciferase over Renilla luciferase activity. Graph was plotted with the mean ± SD of triplicate biological replicates. *, $P < 0.05$; **, $P < 0.01$; ***, $P < 0.001$; ****, $P < 0.0001$.

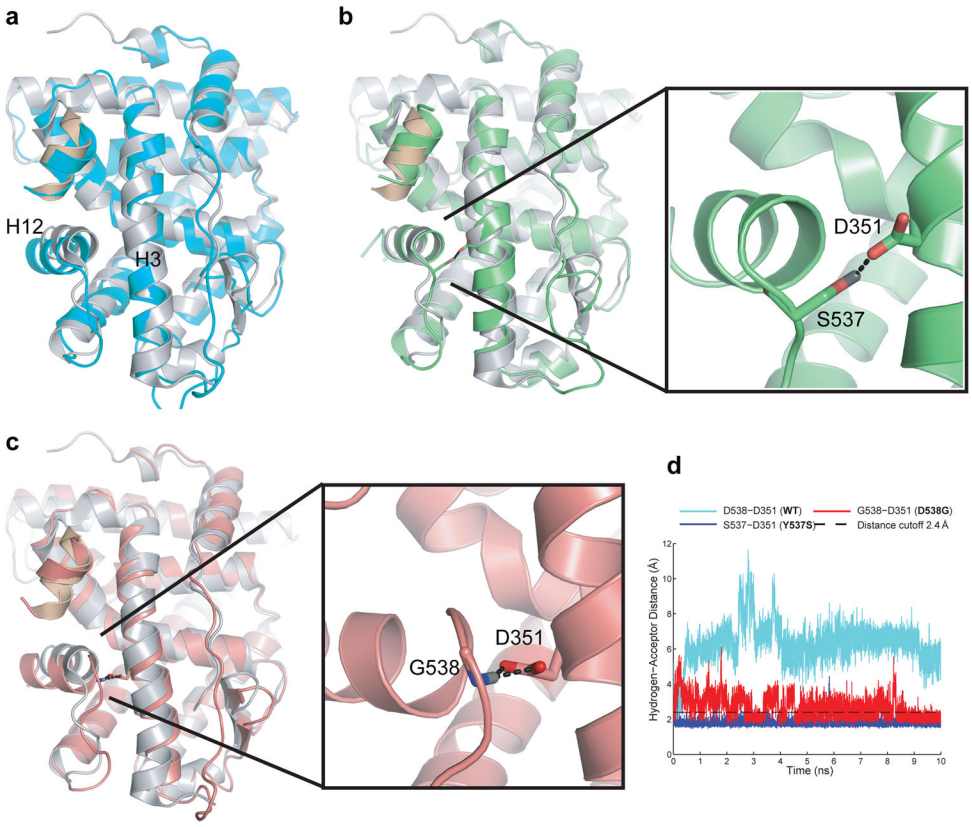

Figure 4. Molecular dynamics-modeled structures of WT and mutant forms of ERα

a. WT (cyan), **b**. Tyr537Ser (green), and **c**. Asp538Gly (red) at 10 ns, overlaid with a co-crystallized structure (PDB accession code 1GWQ) of ERα WT in an agonist conformation (gray) and TIF2 (wheat). **d.** Hydrogen-to-acceptor distances between Asp538/Ser537/Gly538 and Asp351 in ERα WT/Tyr537Ser/Asp538Gly respectively, over the course of 10-ns molecular dynamics simulations.

Table 1

Relationship of *ESR1* mutations to prior hormonal therapy

Case	*ESR1* mutation(s)	Amino acid change(s)	Primary tumor	Mutation Frequency	Duration of hormonal therapies (years)	Types of hormonal therapies given
1	p.Tyr537Ser	Y537S	WT	0.528	2.5	AI, SERM
2	p.Asp538Gly	D538G	WT	0.285	6.5	AI, SERM
3	p.Ser463Pro/ p.Asp538Gly	S463P/D538G	N/A	0.122/0.280	7.5	AI, SERM
4	p.Tyr537Ser/ p.Asp538Gly	Y537S/D538G	N/A	0.082/0.103	3.3	AI, SERD, SERM
5	p.Leu536Arg	L536R	N/A	0.114	10	AI, SERM
6	p.Val534Glu	V534E	N/A	0.056	5.5	AI, SERD
7	p.Tyr537Asn	Y537N	N/A	0.839	5.5	AI, SERM
8	p.Tyr537Ser	Y537S	N/A	0.253	1.5	AI, SERD
9	p.Tyr537Ser	Y537S	N/A	0.265	2.0	AI, SERM, SERD

WT: wild type; N/A: Not available; AI: Aromatase inhibitor; SERM: Selective estrogen receptor modulator; SERD: Selective estrogen receptor degrader.

Table 2

ESR1 mutations among metastatic samples from the BOLERO-2 clinical trial.

Case	*ESR1* Mutation(s)	Amino acid change(s)	Mutation Frequency	Duration prior AI therapy (years)	ER domain
1	p.Ser463Pro/ p.Tyr537Asn	S463P/Y537N	0.18/0.10	2.0	LBD/AF-2
2	p.Pro535His	P535H	0.22	5.0	LBD/AF-2
3	p.Tyr537Cys	Y537C	0.75	3.0	LBD/AF-2
4	p.Tyr537Ser	Y537S	0.09	5.0	LBD/AF-2
5	p.Asp538Gly	D538G	0.13	6.0	LBD/AF-2

N/A: Not available